Research Square

Preprints are preliminary reports that have not undergone peer review.
They should not be considered conclusive, used to inform clinical practice,
or referenced by the media as validated information.

Chemical equilibrium constants of diatomic molecules from a q-deformed hyperbolic interaction potential

E. S. Eyube

edwineyubes@mau.edu.ng

Modibbo Adama University of Technology

D. Festus

Taraba State College of Education

A. Zakariya

Federal College of Education

Saïdou Alioum

University of Maroua

P. A. Njidda

Modibbo Adama University of Technology

I. Joel

Modibbo Adama University of Technology

T. G. Nyagong

Modibbo Adama University of Technology

J. Abe

Modibbo Adama University of Technology

Research Article

Keywords: Diatomic molecules, q-deformed potential, Vibrational energy, Partition function, Gibbs free energy, Chemical equilibrium

Posted Date: September 28th, 2026

DOI: https://doi.org/10.21203/rs.3.rs-10976676/v1

License: This work is licensed under a Creative Commons Attribution 4.0 International License.
Read Full License

Additional Declarations: No competing interests reported.

Chemical equilibrium constants of diatomic molecules from a q-deformed hyperbolic interaction potential

E. S. Eyube[1a*], D. Festus[2b], A. Zakariya[3c], Saïdou Alioum[4d], P. A. Njidda[5e], I. Joel[1f], T. G. Nyagong[6g], J. Abe[1h]

[1]Department of Physics, Faculty of Physical Sciences, Modibbo Adama University, P.M.B. 2076, Yola, Adamawa State, Nigeria.
[2]Department of Physics, College of Education, P.O. Box. 1021, Zing, Taraba State, Nigeria
[3]Department of Physics, Federal College of Education, P.M.B. 2042, Yola, Adamawa State, Nigeria
[4]Department of Physics, Faculty of Science, The University of Maroua, P.O. Box 814, Maroua, Cameroon
[5]Department of Science Policy and Innovation Studies, National Center of Technology Management, Federal Ministry of Innovation, Science and Technology, Modibbo Adama University, P.M.B. 2076, Yola, Adamawa State, Nigeria
[6]Department of Physical Science Education, Faculty of Education, Modibbo Adama University, P.M.B. 2076, Yola, Adamawa State, Nigeria
[*]Corresponding author: [a]Email: edwineyubes@mau.edu.ng: ORCID: 0000-0001-5059-0393

[b]Email: ibwijen5@gmail.com: ORCID: 0009-0000-4617-4733

[c]Email: zkryadamu2@gmail.com: ORCID: 0009-0007-1154-511X

[d]Email: saidoualioum92@gmail.com

[e]Email: patrickabbanjidda@gmail.com: ORCID: 0009-0009-1195-6458

[f]Email: iliyajoel5@gmail.com: ORCID: 0009-0002-1524-9944

[g]Email: timothygregorynyagong@gmail.com: ORCID: 0009-0007-3150-768X

[h]Email: abejessy2020@gmail.com: ORCID: 0009-0002-8871-9126

Abstract

Context: Chemical equilibrium constants depend on the molecular energy levels that determine the partition functions and Gibbs free energies of the reacting species. This study employs a q-deformed hyperbolic interaction potential (qHIP) to calculate the chemical equilibrium constants for the formation of BrF, ClF, IF, and SO from their homonuclear reactants. The qHIP parameters are related to the equilibrium bond length, dissociation energy, and vibrational wavenumber. The calculated chemical equilibrium constants are compared with NIST-JANAF values over 300-6000 K. The average relative absolute deviations are 0.345% for BrF over 300-6000 K, 0.751% for ClF over 300-4600 K, 0.871% for IF over 400-6000 K, and 0.905% for SO over 900-6000 K. ClF exhibits increasing deviations above 4600 K, whereas the largest discrepancies for SO occur below 900 K. These results specify the temperature intervals over which the qHIP-derived equilibrium constants agree closely with NIST-JANAF data.

Methods: The radial Schrödinger equation containing the qHIP was solved using the parametric Nikiforov-Uvarov method to obtain the vibrational energy eigenvalues. The qHIP parameters were

determined from the equilibrium bond length, dissociation energy, and vibrational wavenumber by imposing equilibrium, dissociation, and curvature conditions on the potential. The vibrational energy eigenvalues were used to construct the vibrational partition function, with a molecule-dependent correction parameter determined from Gibbs free-energy data. The vibrational contribution was combined with the rotational and translational partition functions to calculate the molecular Gibbs free energies. Gibbs free-energy changes for the formation of BrF, ClF, IF, and SO were then used to determine their chemical equilibrium constants. The calculated values were assessed against NIST-JANAF data using the relative absolute deviation and average relative absolute deviation. The radial Schrödinger equation containing the qHIP was solved using the parametric Nikiforov-Uvarov method to obtain the vibrational energy eigenvalues. The qHIP parameters were determined from the equilibrium bond length, dissociation energy, and vibrational wavenumber by imposing equilibrium, dissociation, and curvature conditions on the potential. The vibrational energy eigenvalues were used to construct the vibrational partition function, with a molecule-dependent correction parameter determined from Gibbs free-energy data. The vibrational contribution was combined with the rotational and translational partition functions to calculate the molecular Gibbs free energies. Gibbs free-energy changes for the formation of BrF, ClF, IF, and SO were then used to determine their chemical equilibrium constants. The calculated values were assessed against NIST-JANAF data using the relative absolute deviation and average relative absolute deviation.

Keyword: Diatomic molecules; q-deformed potential; Vibrational energy; Partition function; Gibbs free energy; Chemical equilibrium

1. Introduction

Potential energy functions constitute one of the fundamental pillars of molecular quantum mechanics and chemical physics, providing the link between microscopic atomic interactions and experimentally observable molecular properties [1]. Their ability to describe the variation of interaction energy with internuclear separation makes them indispensable for understanding the structural, spectroscopic, dynamical, and thermodynamic behaviour of molecular systems [[1], [2], [3]]. Accurate molecular interaction potentials underpin the prediction of vibrational and rotational energy levels, equilibrium geometries, force constants, dissociation energies, and temperature-dependent thermodynamic properties that are fundamental to chemistry, physics, materials science, atmospheric science, astrophysics, and combustion research [[1], [2], [3], [4]]. They also provide the molecular energy information required for statistical-mechanical calculations of partition functions, Gibbs free energies, and chemical equilibrium constants, thereby establishing a direct link between molecular quantum mechanics and macroscopic chemical behaviour [[5], [6], [7], [8]]. Consequently, the development of reliable interaction potentials remains a central objective of chemical physics, since the predictive capability of molecular theories depends critically on the representation of internuclear interactions [[1], [3]].

The continuing quest for increasingly accurate descriptions of molecular interactions has stimulated the development of numerous analytical and semi-analytical potential energy models over the past several decades [[1], [2], [3]]. This sustained effort reflects the absence of a universal interaction potential capable of accurately reproducing the diverse physical properties of molecular systems [1]. An effective molecular potential should realistically describe the equilibrium configuration, anharmonicity, short-range repulsion, long-range behaviour, and dissociation characteristics while remaining sufficiently simple for analytical treatment or computationally efficient numerical implementation [[1], [9]]. Consequently, a wide range of interaction models has been proposed to improve the prediction of molecular spectra, thermodynamic properties, reaction dynamics, and equilibrium-related quantities [[4], [10], [11], [12], [13]]. The continued evolution of these models reflects the need to balance physical realism with mathematical simplicity, computational efficiency, and predictive accuracy, thereby motivating the ongoing development of improved molecular interaction potentials.

To accommodate the diverse characteristics of molecular interactions, numerous potential energy models have been developed based on different physical assumptions and mathematical formulations [1]. Early interaction potentials, notably the Morse and Kratzer models, established the foundation for analytical descriptions of molecular vibrations and stimulated subsequent developments in molecular

quantum mechanics [[2], [9]]. Continued efforts to improve the representation of anharmonicity and molecular interactions led to increasingly flexible models, including the Deng-Fan, Tietz, improved Tietz, Rosen-Morse, Eckart, Manning-Rosen, Pöschl-Teller, Scarf, Frost-Musulin, and related deformation-based interaction potentials [[14], [15], [16], [17], [18], [19], [20], [21], [22], [23], [24]]. Collectively, these models have contributed to the prediction of molecular energy spectra, spectroscopic constants, and thermodynamic properties, demonstrating that the refinement and application of molecular interaction potentials remain active areas of molecular and chemical physics [[4], [9], [10], [11], [12], [13], [14], [15], [16], [17], [18], [19], [20], [21], [22], [23], [24]].

Among the various classes of molecular interaction potentials, hyperbolic interaction models have attracted sustained attention because of their mathematical versatility and their ability to reproduce essential features of molecular interactions within analytically tractable frameworks [[18], [19], [20], [21], [22], [23], [24]]. Their functional forms provide flexibility for representing anharmonic molecular interactions while permitting exact or approximate analytical solutions of the Schrödinger equation for different molecular systems [[19], [20], [21], [22], [23], [24]]. Consequently, these models have been applied to molecular energy spectra, spectroscopic constants, and thermodynamic properties [[10], [11], [12], [13], [23], [24]]. Their versatility, together with advances in analytical solution techniques, continues to support their application in quantum-mechanical and statistical-mechanical investigations of molecular systems.

Beyond their traditional applications in molecular spectroscopy, molecular interaction potentials have become increasingly important in statistical thermodynamics because they provide the energy spectra required for constructing molecular partition functions and evaluating macroscopic thermodynamic properties [[5], [10], [11], [12], [13], [25], [26], [27], [28], [29], [30], [31]]. Within this framework, the vibrational energy spectrum obtained from an appropriate interaction potential provides molecular-level information for determining temperature-dependent thermodynamic functions through statistical-mechanical formulations [[5], [25], [26], [27], [28], [29], [30], [31]].

Recent studies have further demonstrated this connection for analytically tractable molecular potentials. Oyewumi et al. [10] investigated thermodynamic properties associated with the shifted Deng-Fan potential, while Bakhti et al. [57] employed a q-deformed Scarf-like potential to obtain vibrational partition functions and thermodynamic properties of diatomic molecules. Diaf et al. [58] derived an analytical vibrational partition function for a q-deformed hyperbolic barrier potential and applied the resulting formulation to the thermodynamic properties of diatomic systems. More recently, Ebere et al. [59] investigated the modified shifted Morse potential and obtained partition and related

thermodynamic functions using the Poisson summation approach. Together with other potential-based thermodynamic studies [[11], [12], [13], [25], [26], [27], [28], [29], [30], [31]], these investigations demonstrate the continuing utility of analytical molecular potentials for connecting molecular energy spectra with statistical thermodynamic quantities.

In recent years, this molecular-potential approach has been extended from the calculation of thermodynamic functions to the statistical-mechanical determination of chemical equilibrium constants for gaseous systems [[7], [8], [32], [33], [34], [35]]. Molecular energy levels obtained from analytical interaction models are used to construct partition functions and evaluate Gibbs free energies, from which equilibrium constants can be determined using established thermodynamic relationships [[5], [6], [7], [8], [32], [33], [34], [35]]. Applications to different molecular reactions have demonstrated the feasibility of obtaining equilibrium behaviour from molecular-level energy descriptions [[7], [8], [32], [33], [34], [35]]. This extension is particularly relevant because it carries the information contained in an analytical molecular potential beyond molecular spectra and individual thermodynamic functions to the prediction of chemical reaction equilibrium.

Within this context, q-deformed interaction potentials provide analytically tractable descriptions of anharmonic molecular systems and have been investigated for molecular spectra and thermodynamic properties [[19], [20], [21], [22], [23], [24], [57], [58]]. However, comparatively limited attention has been given to carrying such q-deformed molecular descriptions through the partition function and Gibbs free energy to the prediction of chemical equilibrium constants. Establishing this connection provides a means of assessing whether the molecular energy information generated by a q-deformed interaction model can reproduce reference equilibrium behaviour over extended temperature intervals.

The present work therefore develops a statistical-mechanical framework based on a q-deformed hyperbolic interaction potential (qHIP) for predicting the chemical equilibrium constants of selected diatomic molecular systems. Analytical vibrational energy eigenvalues are employed to construct the molecular partition function and evaluate Gibbs free energies. The potential parameters are related to measurable molecular constants through equilibrium, dissociation, and curvature conditions, thereby adapting the interaction model to individual molecular systems. Chemical equilibrium constants are subsequently obtained for BrF, ClF, IF, and SO and compared with NIST-JANAF thermochemical data over broad temperature intervals. This treatment extends the application of the qHIP from the molecular energy description to reaction-equilibrium thermodynamics and provides a quantitative assessment of the temperature ranges over which the resulting molecular model reproduces reference equilibrium behaviour.

2. Theoretical formulation

This section presents the theoretical formulation based on the q-deformed hyperbolic interaction potential

$$\mathrm{U}(r)=\mathrm{U}_0\frac{\cosh_q^2\left(\frac{1}{2}\alpha r\right)}{\cosh^2\left(\frac{1}{2}\alpha r\right)}, \tag{1}$$

where U_0 denotes the interaction strength, α is the screening parameter governing the interaction range, q is the deformation parameter, and r represents the internuclear separation. Based on this interaction model, analytical expressions are developed for the vibrational energy eigenvalues, molecular partition function, Gibbs free energy, and chemical equilibrium constants.

2.1.Vibrational energy eigenvalues

For the determination of the vibrational energy eigenvalues, only the vibrational motion of the system is considered. The rotational contribution is included separately in the molecular partition function; consequently, the centrifugal term is omitted. The radial Schrödinger equation is then written as

$$\left[-\frac{\hbar^2}{2\mu}\frac{\mathrm{d}^2}{\mathrm{d}r^2}+\mathrm{U}(r)\right]\mathrm{y}_v(r)=E_v\mathrm{y}_v(r), \tag{2}$$

where μ is the reduced mass of the diatomic molecule, v is the vibrational quantum number (v = 0, 1, 2, …), $\hbar$ is the reduced Planck constant, E_v is the vibrational energy eigenvalue, and $\mathrm{y}_v(r)$ is the corresponding vibrational wave function. To obtain an explicit expression for E_v from Eqs. (1) and (2), the parametric Nikiforov-Uvarov solution (PNUS) approach is employed. In the PNUS approach, a suitable change of variable reduces the radial Schrödinger equation to the hypergeometric-type differential equation [36]

$$\frac{\mathrm{d}^2\mathrm{y}_v(x)}{\mathrm{d}x^2}+\frac{b_1-b_2x}{x(1-b_3x)}\frac{\mathrm{d}\mathrm{y}_v(x)}{\mathrm{d}x}+\frac{-c_1x^2+c_2x-c_v}{x^2(1-b_3x)^2}\mathrm{y}_v(x)=0, \tag{3}$$

where b_1, b_2, c_1, c_2, and c_3 are constants. The energy eigenvalue equation is

$$b_3v^2+(b_2-b_3)v-(2v+1)b_5+(2v+1)\left(\sqrt{b_9}+b_3\sqrt{b_8}\right)+b_7+2b_3b_8+2\sqrt{b_8b_9}=0, \tag{4}$$

where

$$\begin{aligned} &b_4=\tfrac{1}{2}(1-b_1),\quad b_5=\tfrac{1}{2}(b_2-2b_3),\quad b_6=b_5^2+c_1\\ &b_7=2b_4b_5-c_2,\quad b_8=b_4^2+c_v,\quad b_9=b_6+b_3b_7+b_3^2b_8 \end{aligned}. \tag{5}$$

Combining Eqs. (1) and (2) and applying the transformation $x=\left(1+\mathrm{e}^{\alpha r}\right)^{-1}$ gives

$$\frac{\mathrm{d}^2\mathrm{y}_\nu(x)}{\mathrm{d}x^2}+\frac{1-2x}{x(1-x)}\frac{\mathrm{dy}_\nu(x)}{\mathrm{d}x}+\frac{-c_1x^2+c_2x-c_\nu}{x^2(1-x)^2}\mathrm{y}_\nu(x)=0, \tag{6}$$

where $c_1=\frac{2\mu}{\alpha^2\hbar^2}\mathrm{U}_0(q-1)^2$, $c_2=-\frac{4\mu}{\alpha^2\hbar^2}\mathrm{U}_0(q-1)$, and $c_\nu=\frac{2\mu}{\alpha^2\hbar^2}(\mathrm{U}_0-E_\nu)$.

Comparison of Eqs. (6) and (3) gives $b_1=1$, $b_2=2$, $b_3=1$. Using these values in Eq. (5) gives $b_4=0$, $b_5=0$, $b_6=c_1$, $b_7=-c_2$, $b_8=c_\nu$ and $b_9=c_1-c_2+c_\nu$. Their replacement into Eq. (4) gives the vibrational energy eigenvalue equation

$$E_\nu=\mathrm{U}_0-\frac{\alpha^2\hbar^2}{8\mu}\left\{\nu+\frac{1}{2}-\sqrt{\frac{2\mu}{\alpha^2\hbar^2}\mathrm{U}_0(q-1)^2+\frac{1}{4}}-\frac{\frac{2\mu}{\alpha^2\hbar^2}\mathrm{U}_0(q^2-1)}{\nu+\frac{1}{2}-\sqrt{\frac{2\mu}{\alpha^2\hbar^2}\mathrm{U}_0(q-1)^2+\frac{1}{4}}}\right\}^2. \tag{7}$$

Equation (7) provides the energy spectrum required for constructing the vibrational contribution to the molecular partition function.

2.2.Partition function and Gibbs free energy

For a diatomic molecule in the ideal-gas state, the molecular partition function comprises the vibrational, rotational, and translational contributions [[5], [37]]

$$\mathrm{Q}=\mathrm{Q_a}\mathrm{Q_b}\mathrm{Q_c}, \tag{8}$$

where $\mathrm{Q_a}$, $\mathrm{Q_b}$, and $\mathrm{Q_c}$ denote the vibrational, rotational, and translational partition functions, respectively.

The vibrational contribution is developed from the energy eigenvalues in Eq. (7). For discrete vibrational states, the conventional form of the vibrational partition function is $\mathrm{Q_a}=\sum_{\nu=0}^{\nu_{\max}}\exp(-\beta E_\nu)$ [[5], [37]], where $\beta=(\mathrm{k_B}T)^{-1}$, $\mathrm{k_B}$ is the Boltzmann constant, T is the absolute temperature, and $\nu_{\max}$ is the maximum vibrational quantum number associated with the upper bound of the vibrational spectrum. The value of $\nu_{\max}$ follows from the stationary condition $\partial E_\nu/\partial\nu\big|_{\nu=\nu_{\max}}=0$, giving $\nu_{\max}=\Lambda_1-\Lambda_2$, where $\Lambda_1=-\frac{1}{2}+\sqrt{\frac{2\mu}{\alpha^2\hbar^2}\mathrm{U}_0(q-1)^2+\frac{1}{4}}$ and $\Lambda_2=\sqrt{\frac{2\mu}{\alpha^2\hbar^2}\mathrm{U}_0(q^2-1)}$.

Although the energy eigenvalues in Eq. (7) describe the pure vibrational motion associated with the qHIP, molecule-specific effects beyond this description can contribute to the vibrational thermodynamics. In particular, higher-order anharmonicity and coupling between vibrational and rotational motions are not explicitly contained in the derived spectrum. Their combined influence is represented by a dimensionless correction parameter η, introduced as a multiplicative factor in Q_a. For each molecule, η is determined by minimizing the average relative absolute deviation (ARAD) between the calculated and reference Gibbs free energies over the temperature interval considered. The corrected vibrational partition function then takes the form

$$Q_a = \exp(-\eta)\sum_{v=0}^{v_{max}} \exp(-\beta E_v). \tag{9}$$

Combining the energy spectrum in Eq. (7) with Eq. (9) leads to

$$Q_a = \exp(-\beta U_0 - \eta)\sum_{v=0}^{v_{max}} \lambda_v, \tag{10}$$

where $\lambda_v = \exp\left\{\kappa\left(v - \Lambda_1 - \frac{\Lambda_2^2}{v-\Lambda_1}\right)\right\}^2$ and $\kappa = \frac{1}{2}\alpha\hbar\left(\frac{1}{2}\beta\mu^{-1}\right)^{\frac{1}{2}}$. The finite sum in Eq. (10) is evaluated using the Poisson summation method. Over the interval from v = 0 to v_{max}, the corresponding expression is [38]

$$\sum_{v=0}^{v_{max}} \lambda_v = \frac{1}{2}\lambda_0 - \frac{1}{2}\lambda_{v_{max}+1} + \sum_{j=-\infty}^{j=+\infty} \int_0^{v_{max}+1} \lambda_v \exp(-i2\pi j v)\,dv. \tag{11}$$

Under the classical-limit approximation, only the $j = 0$ Fourier mode is retained, reducing Eq. (11) to

$$\sum_{v=0}^{v_{max}} \lambda_v \approx \frac{1}{2}\lambda_0 - \frac{1}{2}\lambda_{v_{max}+1} + \int_0^{v_{max}+1} \lambda_v\,dv, \tag{12}$$

whereas the nonzero modes ($j \neq 0$) generate oscillatory integrals that do not admit closed analytical forms. The same j = 0 truncation has been adopted in Refs. [[39], [40]], where inclusion of the remaining Fourier modes likewise prevents an analytical reduction of the partition function.

Introducing the expression for λ_v into Eq. (12) leads to

$$\sum_{v=0}^{v_{max}} \lambda_v \approx \frac{1}{2}\exp(\lambda_1^2) - \frac{1}{2}\exp(\lambda_2^2) + \frac{\sqrt{\pi}}{2\kappa}\{\mathrm{Erfi}(\lambda_1) + \mathrm{Erfi}(\lambda_2)\} + \frac{1}{2\kappa}\int_{-\lambda_1}^{\lambda_2} \frac{p\exp(p^2)\,dp}{\sqrt{p^2 + 4\kappa^2\Lambda_2^2}}, \tag{13}$$

where $\lambda_1 = \kappa\left(\Lambda_1 - \Lambda_1^{-1}\Lambda_2^2\right)$, $\lambda_2 = \kappa\left[\nu_{\max} + 1 - \Lambda_1 - \left(\nu_{\max} + 1 - \Lambda_1\right)^{-1}\Lambda_2^2\right]$, $p = \lambda_\nu^{\frac{1}{2}}$, and Erfi($x$) denotes the imaginary error function evaluated at x. The integral appearing in Eq. (13) has been shown to make a negligible contribution for molecular parameters of diatomic systems [41]. Omitting this term and carrying the remaining terms into Eq. (10) produces

$$\mathrm{Q_a} = \frac{1}{2}\exp\left(\lambda_1^2 - \beta \mathrm{U}_0 - \eta\right) - \frac{1}{2}\exp\left(\lambda_2^2 - \beta \mathrm{U}_0 - \eta\right) + \frac{\sqrt{\pi}}{2\kappa}\exp\left(-\beta \mathrm{U}_0 - \eta\right)\left\{\mathrm{Erfi}\left(\lambda_1\right) + \mathrm{Erfi}\left(\lambda_2\right)\right\}. \quad (14)$$

Equation (14) is the analytical vibrational partition function associated with the qHIP.

Having established the vibrational contribution, the rotational contribution to the molecular partition function is [42]

$$\mathrm{Q_b} = \frac{1}{s}\left(\frac{1}{\beta_\mathrm{b}} + \frac{1}{3} + \frac{\beta_\mathrm{b}}{15} + \frac{4\beta_\mathrm{b}^2}{315}\right), \quad (15)$$

where s is the symmetry number, with $s = 1$ for heteronuclear molecules and $s = 2$ for homonuclear molecules, while $\beta_\mathrm{b} = \beta\hbar^2/2\pi r_\mathrm{e}^2$ represents the characteristic rotational temperature. The translational contribution takes the form [42]

$$\mathrm{Q_c} = \left(\frac{m}{2\pi\hbar^2\beta}\right)^{\frac{3}{2}}\frac{1}{P\beta}, \quad (16)$$

where m is the mass of a single molecule and P is the pressure. Equations (14)– (16) complete the vibrational, rotational, and translational contributions required in Eq. (8). The resulting molecular partition function is then used to evaluate the Gibbs free energy according to [42]

$$\mathrm{G} = -\mathrm{R}T\ln\mathrm{Q}, \quad (17)$$

where R is the universal gas constant.

2.3.Chemical equilibrium constant

The chemical equilibrium constant is formulated by considering the reversible formation of a heteronuclear diatomic molecule from two distinguishable atomic species

$$\tfrac{1}{2}\mathrm{X}_2 + \tfrac{1}{2}\mathrm{Y}_2 \rightleftharpoons \mathrm{XY}, \quad (18)$$

where X and Y represent the constituent atomic species. The Gibbs free-energy change associated with the reaction in Eq. (18) is written as

$$\Delta G_{XY} = G_{XY}^{TOT} - \frac{1}{2} G_{X_2}^{TOT} - \frac{1}{2} G_{Y_2}^{TOT}, \tag{19}$$

where G_j^{TOT} denotes the total Gibbs free energy of species *j*. The total Gibbs free energy of each species is written as [7]

$$G_j^{TOT} = G_j + \Delta_f H_j^0 - H_j^0. \tag{20}$$

where G_j is the molar Gibbs free energy, H_j^0 is the sensible molar enthalpy at the reference state, and $\Delta_f H_j^0$ is the standard enthalpy of formation of species *j*. The sensible molar enthalpy is calculated from the molecular partition function according to [7]

$$H = -N_A \frac{\partial}{\partial \beta} \ln Q, \tag{21}$$

where N_A is the Avogadro constant. The value of H_j^0 is obtained from Eq. (21) at $T = 298.15$ K and $P = 1$ atm, whereas $\Delta_f H_j^0$ at the same reference state is taken from available reference thermochemical data [6]. The chemical equilibrium constant is related to the Gibbs free-energy change through the thermodynamic relation [7]

$$\Delta G_{XY} = -RT \ln K_P. \tag{22}$$

3. Results and discussion

The molecular systems considered in the present calculations comprise BrF, ClF, IF, and SO together with their corresponding homonuclear reactant species. The molecular constants r_e, D_e, and ω_e for the reactant and product species were obtained from Refs. [[43], [44], [45], [46], [47], [48], [49], [50], [51], [52]], as indicated individually in Table 1. The table also presents the reference-state enthalpies and model parameters required for the calculations. These species provide the molecular inputs required to implement the general equilibrium reaction defined in Eq. (18) and subsequently evaluate the chemical equilibrium constants.

BrF, ClF, and IF belong to the diatomic interhalogen family, whose members are of interest because of the bonding and chemical reactivity associated with combinations of unlike halogen atoms [53]. SO, in contrast, is a sulfur-containing diatomic species of relevance to areas such as combustion,

atmospheric chemistry, and molecular spectroscopy [54]. The inclusion of these chemically different molecular systems provides a basis for examining the applicability of the qHIP to the prediction of their equilibrium properties.

For application to the selected diatomic molecules, the parameters of the qHIP are related to measurable molecular quantities rather than assigned independently. A suitable diatomic interaction potential should possess a minimum at the equilibrium bond length r_e, with the dissociation limit characterized by D_e. Such physical requirements provide constraints through which the parameters of the interaction potential can be obtained from molecular data [55]. Accordingly, the qHIP is subjected to the conditions

$$\mathrm{U}(r_e) = 0, \quad \lim_{r\to\infty} \mathrm{U}(r) = D_e, \quad \mathrm{U}'(r_e) = 0, \quad \mathrm{U}''(r_e) = \mathrm{k}_e, \tag{23}$$

where k_e is the force constant associated with the curvature of the potential at its minimum. Since ω_e in Table 1 is expressed as a spectroscopic wavenumber, the force constant is evaluated from $\mathrm{k}_e = \mu(2\pi c\omega_e)^2$, where μ is the reduced mass and c is the speed of light. Applying the conditions in Eq. (23) to the qHIP in Eq. (1) gives $q = -\exp(p)$ and $\mathrm{U}_0 = D_e$, while $p = \alpha r_e$. The curvature condition further gives

$$p = \sqrt{\Delta} + \mathrm{W}\left(\sqrt{\Delta}\exp\left(-\sqrt{\Delta}\right)\right). \tag{24}$$

In this equation, $\Delta = r_e^2\mathrm{k}_e/2D_e$ is the Sutherland dimensionless parameter [56], and W(x) denotes the Lambert W function. The molecular constants listed in Table 1 are therefore used to determine the molecule-specific parameters of the qHIP, thereby linking the analytical interaction model to the equilibrium and spectroscopic characteristics of each molecular species. The resulting values of p are reported in Table 1.

With the qHIP parameters established from the molecular constants, the vibrational partition function in Eq. (14), together with the rotational and translational contributions in Eqs. (15) and (16), was used to evaluate the Gibbs free energy through Eq. (17). The molecule-dependent correction parameter η was determined for each species by minimizing the average relative absolute deviation between the calculated and reference Gibbs free energies over the temperature interval considered, as described in Section 2.2. The resulting values of η are included in Table 1.

The calculated Gibbs free energies provide the quantities required to determine the Gibbs free-energy change in Eq. (19). The reference-state enthalpy terms entering Eq. (20) were incorporated using the

values reported in Table 1, with the sensible molar enthalpy H_j^0 evaluated from Eq. (21) at 298.15 K and the standard enthalpy of formation $\Delta_f \mathrm{H}_j^0$ obtained from reference thermochemical data [6]. The corresponding chemical equilibrium constants were then calculated from Eq. (22).

The calculated chemical equilibrium constants were expressed as $\log_{10} K_p$ and compared with the NIST-JANAF data [6]. The numerical results for BrF, ClF, IF, and SO are presented in Tables 2-5, respectively, while their temperature dependence is shown in Figs. 1-4. The relative absolute deviation (RAD) at each temperature was evaluated from $\mathrm{RAD} = 100\left|1 - X_{\mathrm{cal}} / X_{\mathrm{NIST}}\right|$, where X_{cal} represents the value of $\log_{10} K_p$ obtained in the present work and X_{NIST} is the corresponding NIST-JANAF value. The average relative absolute deviation (ARAD) over the selected temperature interval was calculated from $\mathrm{ARAD} = N^{-1} \sum_{k=1}^{N} \left(\mathrm{RAD}\right)_k$, where N is the number of temperature points included in the averaging.

For BrF, $\log_{10} K_p$ decreases from 13.122 at 300 K to 0.873 at 6000 K, while the corresponding NIST-JANAF values decrease from 12.868 to 0.885. The RAD is 1.974% at 300 K, falls to 0.003% at 400 K, and remains below 1% from 400 to 5700 K before increasing to 1.070%, 1.213%, and 1.313% at 5800, 5900, and 6000 K, respectively. Over the complete temperature interval of 300-6000 K, the ARAD is 0.345%. Figure 1 illustrates the close proximity of the calculated and NIST-JANAF equilibrium constants and the associated variation of RAD with temperature.

For ClF, the calculated $\log_{10} K_p$ decreases from 9.020 at 300 K to 0.675 at 6000 K, compared with NIST-JANAF values of 9.018 and 0.834 at the same temperatures. The RAD increases from 0.017% at 300 K to 0.908% at 2700 K and subsequently decreases to 0.161% at 3700 K. At higher temperatures, the deviation increases, reaching 3.775% at 4600 K and 19.063% at 6000 K. The ARAD evaluated over 300-4600 K is 0.751%. The increasing departure between the qHIP and NIST-JANAF results toward the upper-temperature region is reflected in both $\log_{10} K_p$ and the corresponding RAD shown in Fig. 2.

The IF results exhibit a larger deviation at the lowest temperature considered. At 300 K, the calculated and NIST-JANAF values of $\log_{10} K_p$ are 22.168 and 20.512, respectively, corresponding to a RAD of 8.075%. At 400 K, the RAD decreases to 2.166%, and at 500 K it falls to 0.021%. From 500 K onward, the deviations initially remain small and subsequently increase gradually at higher temperatures, reaching 1.006% at 4500 K and 2.930% at 6000 K. Over the adopted interval of 400-6000 K, the

ARAD is 0.871%. Figure 3 captures this temperature-dependent behaviour, particularly the larger difference at the lower end of the temperature range and the closer agreement obtained thereafter.

A markedly different low-temperature behaviour is obtained for SO. At 300 K, the qHIP and NIST-JANAF values of $\log_{10} K_p$ are 10.593 and 3.689, respectively, giving a RAD of 187.144%. The RAD decreases successively to 106.484%, 65.454%, 39.693%, 21.843%, and 8.603% between 400 and 800 K. At 900 K, the calculated value of 3.709 is close to the NIST-JANAF value of 3.708, corresponding to a RAD of 0.014%. From 900 K onward, the deviations are considerably smaller than those below 900 K, although they increase gradually at higher temperatures and reach 2.140% at 6000 K. The ARAD over 900-6000 K is 0.905%. Figure 4 emphasizes the strong temperature dependence of the SO results, with the pronounced low-temperature departure giving way too much closer agreement from 900 K onward.

The comparison reveals distinct species- and temperature-dependent patterns in the calculated equilibrium constants. BrF maintains relatively small deviations throughout the investigated temperature range, with an ARAD of 0.345% over 300-6000 K. For ClF, the deviation becomes more pronounced at elevated temperatures, although an ARAD of 0.751% is obtained over 300-4600 K. The IF results show their largest departure at 300 K, followed by considerably smaller deviations from 400 K onward, giving an ARAD of 0.871% over 400-6000 K. In contrast, SO exhibits substantial deviations below 900 K but much closer agreement at higher temperatures, with an ARAD of 0.905% over 900-6000 K. These temperature-dependent differences define the ranges within which the qHIP-based formulation provides a consistent description of the NIST-JANAF equilibrium data and identify the temperature regions where larger departures from the reference values occur.

4. Conclusions

The q-deformed hyperbolic interaction potential was employed to obtain the vibrational energy spectrum and formulate the molecular partition function for evaluating the thermodynamic properties of selected diatomic systems. The potential parameters were related to the molecular constants r_e, D_e, and ω_e by imposing the equilibrium, dissociation, and curvature conditions appropriate to a diatomic molecular potential. The resulting formulation was subsequently used to calculate the Gibbs free energies and chemical equilibrium constants for the formation of BrF, ClF, IF, and SO from their corresponding homonuclear species. Comparison of the calculated $\log_{10} K_p$ values with NIST-JANAF data gave ARAD values of 0.345% for BrF over 300-6000 K, 0.751% for ClF over 300-4600 K, 0.871% for IF over 400-6000 K, and 0.905% for SO over 900-6000 K. The results also reveal temperature-dependent departures outside some of these intervals, particularly for ClF at higher temperatures and SO below 900 K. Within the stated temperature ranges, the calculated equilibrium constants reproduce the reference data with small average deviations, while the departures observed beyond these ranges indicate the temperature limits of the present formulation.

Statements and Declarations

Funding: This research received no external funding.

Competing Interests: The authors declare that they have no known competing financial or non-financial interests, or personal relationships that could have appeared to influence the work reported in this paper.

Data Availability: All data generated or analyzed during this study are presented in the manuscript. The study is based on analytical and computational procedures. No new experimental datasets were generated, and no datasets were deposited in a public repository. Reference thermochemical data used for comparison are cited in the manuscript.

Code Availability: Not applicable.

Author Contributions: E. S. Eyube: Conceptualization, Formal analysis, Methodology, Project administration, Resources, Software, Supervision, Validation, Visualization, Writing-original draft, Writing-review and editing. D. Festus: Data curation, Formal analysis, Investigation, Methodology, Resources, Software, Writing-original draft, Writing-review and editing. A. Zakariya: Data curation, Formal analysis, Investigation, Methodology, Resources, Visualization, Writing-original draft, Writing-review and editing. Saïdou Alioum: Data curation, Formal analysis, Investigation, Methodology, Resources, Visualization, Writing-original draft, Writing-review and editing. P. A. Njidda: Data curation, Formal analysis, Investigation, Methodology, Resources, Software, Writing-original draft, Writing-review and editing. I. Joel: Data curation, Formal analysis, Investigation, Methodology, Software, Visualization, Writing-original draft, Writing-review and editing. T. G. Nyagong: Data curation, Formal analysis, Investigation, Methodology, Resources, Software, Writing-original draft, Writing-review and editing. J. Abey: Data curation, Formal analysis, Investigation, Methodology, Resources, Visualization, Writing-original draft, Writing-review and editing.

Ethics Approval: Not applicable.

Consent to Participate: Not applicable.

Consent for Publication: Not applicable.

Final Approval of Manuscript: All authors have read and approved the final version of the manuscript and agree to its submission for publication.

References

[1] J.P. Araùjo, M.Y. Ballester, A comparative review of 50 analytical representation of potential energy interaction for diatomic systems: 100 years of history, *Int. J. Quantum Chem*. 121 (2021) e26808. https://doi.org/10.1002/qua.26808

[2] P.M. Morse, Diatomic molecules according to the wave mechanics. II. vibrational levels, *Phys. Rev*. 34 (1929) 57. https://doi.org/10.1103/PhysRev.34.57

[3] P. Schwerdtfeger, D.J. Wales, 100 years of the Lennard-Jones potential, *J. Chem. Theory Comput*., 20 (2024) 3379. https://doi.org/10.1021/acs.jctc.4c00135

[4] A.D. Ahmed, E.S. Eyube, E. Omugbe, C.A. Onate, P. Timtere, Bound-state energy spectrum and thermochemical functions of the deformed Schiöberg oscillator, *Sci. Rep*. 13 (2023) 20386. https://doi.org/10.1038/s41598-023-47235-0

[5] P.S. Barklem, R. Collet, Partition functions and equilibrium constants for diatomic molecules and atoms of astrophysical interest, *A&A* 588 (2016) A96. https://doi.org/10.1051/0004-6361/201526961

[6] M.W. Chase, NIST-JANAF Thermochemical Tables, 4th Edition, American Institute of Physics, New York 1988. https://doi.org/10.18434/T42S31

[7] Wang C.W., Peng X.L., Liu J.Y., Jiang R., Li X.P., Liu Y.S., Liu S.Y., Wei L.S., Zhang L.H. and Jia C.S., A novel formulation representation of the equilibrium constant for water gas shift reaction, *Int. J. Hydrogen Energy,* 47 (2022) 27821. https://doi.org/10.1016/j.ijhydene.2022.06.105

[8] Eyube E.S., Musa R.D., Ayuba J.B., Omugbe E., Onate C.A., Joel I., Shittu M., and Musa Y.D., Equilibrium constants of NO, PO and PN from an improved Frost-Musulin potential, *Chem. Phys. Lett*. 893 (2026) 142839. https://doi.org/10.1016/j.cplett.2026.142839

[9] A. Mirzanejad, S.A. Varganov, Derivation of Morse potential, *Mol. Phys*. 123 (2025) e2360542. https://doi.org/10.1080/00268976.2024.2360542

[10] Oyewumi K.J., Falaye B.J., Onate C.A., Oluwadare O.J., Yahya W.A., Thermodynamic properties and the approximate solutions of the Schrödinger equation with the shifted Deng-Fan potential model, *Mol. Phys*. 112 (2014) 127. https://doi.org/10.1080/00268976.2013.804960

[11] Ghanbari A., Khordad R., Thermodynamic properties of several substances using Tietz-Hua potential, *Indian J. Phys*. 96 (2022) 1413. https://doi.org/10.1007/s12648-021-02086-1

[12] Fan Z., Wang Y., Tian H., Ni Z., Fan Q., Li H., Fu J., Ma J., Xie F., Thermodynamic properties of carbon monoxide using an improved Hulburt-Hirschfelder potential, *Int. J. Thermophys*. 44 (2023) 22. https://doi.org/10.1007/s10765-022-03091-0

[13] Onate C.A., Okon I.B., Omugbe E., Eyube E.S., Al-Asbahi B.A., Kumar Y.A., Emeje K.O., Aghemenloh E., Obasuyi A.R., Obaje V.O. Etchie T.O., Theoretical prediction of molar entropy of modified shifted Morse potential for gaseous molecules. *Chem. Phys*. 582 (2024) 112294. https://doi.org/10.1016/j.chemphys.2024.112294

[14] H. Hassanabadi, B.H. Yazarloo, S. Zarrinkamar, H. Rahimov, Deng-Fan potential for relativistic spinless particles - an ansatz solution, *Commun. Theor. Phys*. 57 (2012) 339. https://doi.org/10.1088/0253-6102/57/3/02

[15] H. Hassanabadi, E. Maghsoodi, S. Zarrinkamar (2012). Relativistic symmetries of Dirac equation and the Tietz potential. *Eur. Phys. J. Plus* 127: 31. https://doi.org/10.1140/epjp/i2012-12031-1

[16] C.S. Jia, Y.F. Diao, X.J. Liu, P.Q. Wang, J.Y. Liu, G.D. Zhang, Equivalence of the Wei potential model and Tietz potential model for diatomic molecules, J. Chem. Phys. 137 (2012) 014101. https://doi.org/10.1063/1.4731340

[17] H.M. Tang, G.C. Liang, L.H. Zhang, F. Zhao, C.S. Jia, Molecular energies of the improved Tietz potential energy model, *Can. J. Chem*. 92 (2014) 201. https://doi.org/10.1139/cjc-2013-0466

[18] N. Rosen and Philip M. Morse, On the vibrations of polyatomic molecules, Phys. Rev. 42 (1932) 210. https://doi.org/10.1103/PhysRev.42.210

[19] G. Pöschl, E. Teller, Bemerkungen zur Quantenmechanik des anharmonischen Oszillators. *Z. Physik* 83:143. https://doi.org/10.1007/BF01331132 (1933).

[20] G.F. Wei, S.H. Dong, Approximately analytical solutions of the Manning-Rosen potential with the spin-orbit coupling term and spin symmetry, *Phys. Lett. A* 373 (2008) 49. https://doi.org/10.1016/j.physleta.2008.10.064

[21] G. L´evai, M. Znojil, The interplay of supersymmetry and PT symmetry in quantum mechanics: a case study for the Scarf II potential, *J. Phys. A: Math. Gen*. 35 (2002) 8793. https://doi.org/10.1088/0305-4470/35/41/311

[22] A.A. Frost, B. Musulin, Semiempirical potential energy functions. I. The H_2 and H_2^+ diatomic molecules, *J. Chem. Phys*. 22 (1954) 1017. https://doi.org/10.1063/1.1740254

[23] I.J. Njoku, E. Onyeocha, P. Nwaokafor, M. Onuoha, Energy eigenvalues of diatomic molecules with the shifted Deng-Fan potential using a recently introduced approximation scheme, *Chem. Phys. Impact* 5 (2022) 100096. https://doi.org/10.1016/j.chphi.2022.100096

[24] E. Omugbe, R. Horchani, N.J. Okoro, E.S. Eyube, C.A. Onate, E.P. Inyang, V.C. Eze, E. Feddi, Non-relativistic energy spectra of and diatomic molecules confined in a modified Scarf potential via supersymmetric WKB approach, *Mol. Phys*. 123 (2025) e2390591. https://doi.org/10.1080/00268976.2024.2390591

[25] Wang J., Jia C.S., Li C.J., Peng X.L., Zhang L.H., Liu J.Y., Thermodynamic properties for carbon dioxide, *ACS Omega* 4 (2019) 19193. https://doi.org/10.1021/acsomega.9b02488

[26] Wang C.W., Wang J., Liu Y.S., Li J., Peng X.L., Jia C.S., Zhang L.H., Yi L.Z., Liu J.Y., Li C.J., Jia X., Prediction of the ideal-gas thermodynamic properties for water, *J. Mol. Liq*. 321 (2021) 114912. https://doi.org/10.1016/j.molliq.2020.114912

[27] Jia C.S., Li J., Liu Y.S., Peng X.L., Jia X., Zhang L.H., Jiang R., Li X.P., Liu J.Y., Zhao Y.L., Predictions of thermodynamic properties for hydrogen sulfide, *J. Mol. Liq*. 315 (2020) 113751. https://doi.org/10.1016/j.molliq.2020.113751

[28] Liu G.H., Ding D.C., Wang C.W., Jia C.S., Unified non-fitting explicit formulation of thermodynamic properties for five compounds, *J. Mol. Struct*., 1294 (2023) 136543 https://doi.org/10.1016/j.molstruc.2023.136543

[29] Ding Q.C., Jia C.S., Wang C.W., Peng X.L., Liu J.Y., Zhang L.H., Jiang R., Zhu S.Y., Yuan H., Tang H.X., Unified non-fitting formulation representation of thermodynamic properties for diatomic substances, *J. Mol. Liq*., 371 (2023) 121088. https://doi.org/10.1016/j.molliq.2022.121088

[30] Eyube E.S., Onate C.A., Omugbe E., Nwabueze C.M., Theoretical prediction of Gibbs free energy and specific heat capacity of gaseous molecules. *Chem. Phys*. 560 (2022) 111572. https://doi.org/10.1016/j.chemphys.2022.111572

[31] Eyube E.S., Bitrus B.M., Samaila H., Notani P.P., Model entropy equation for gaseous substances, *Int. J. Thermophys*., 43 (2022) 55. https://doi.org/10.1007/s10765-022-02980-8

[32] Wang, C. W., Peng, X. L., Liu, J. Y., Jiang, R., Li, X. P., Liu, Y. S., Liu, S. Y., Wei, L. S., Zhang, L. H., and Jia, C. S., Prediction of chemical equilibrium constants for hydrolysis of COS based on molecular potential models, *Fuel* 362 (2024) 130916. https://doi.org/10.1016/j.fuel.2024.130916

[33] Wang J.F., Zhang H., Liang L.X., Peng X.L., Wang C.W., Deng P., Ding Q.C., and Jia C.S., *Comput. Theor. Chem.*, A novel formulation representation regarding the equilibrium constant subject to reaction between N_2 and O_2, 1239 (2024) 114758. https://doi.org/10.1016/j.comptc.2024.114758

[34] Guo J.J., Ding Q.C., Jia C.S., Zhang L.H., Peng X.L., Wang C.W., Zhao Y.L., Li G., Li X.G., Liu J.Y., Qiu Y., Wu J.J., and Wei L.S., A novel molecular-structure-based formulation representation for the H_2S decomposition reaction equilibrium constant, *Energy,* 314 (2025) 134108. https://doi.org/10.1016/j.energy.2024.134108

[35] Eyube E.S., Musa R.D., Makasson C.R., Onate C.A., Omugbe E., Tahir A.M., Musa Y.D., and Zakariya A., Closed-form partition-function treatment of equilibrium constants in anharmonic diatomic systems, *Chem. Phys*. 610 (2026) 113366. https://doi.org/10.1016/j.chemphys.2026.113366

[36] Tezcan C. and Sever R., A General Approach for the exact solution of the Schrödinger equation. *Int. J. Theor. Phys*. 48 (2009) 337. https://doi.org/10.1007/s10773-008-9806-y

[37] Pathria R.K. and Beale P.D., Statistical Mechanics, 3rd ed. (Elsevier, Oxford, 2011)

[38] Song, X.Q.; Wang, C.W., and Jia, C.S., Thermodynamic properties of the sodium dimer. *Chem. Phys. Lett.* 673 (2017) 50. https://doi.org/10.1016/j.cplett.2017.02.010

[39] Jia C.S., Wang C.W., Zhang L.H., Peng X.L., Zeng R., and You X.T., Partition function of improved Tietz oscillators. *Chem. Phys. Lett.* 676 (2017) 150. https://doi.org/10.1016/j.cplett.2017.03.068

[40] Eyube E.S., Entropy and Gibbs free energy equations for the specialized Pöschl-Teller potential. *Eur. Phys. J. Plus* 137 (2022) 760. https://doi.org/10.1140/epjp/s13360-022-02931-0

[41] Eyube E.S., Notani P.P., Dlama Y., Omugbe E., Onate C.A., Okon I.B., Nyam G.G., Jabil Y.Y., and Izam M.M., Isobaric molar heat capacity model for the improved Tietz potential. *Int. J. Quantum Chem.* 123 (2022) e27040. https://doi.org/10.1002/qua.27040

[42] Peng X.L., Jiang R., Jia C.S., Zhang L.H., and Zhao Y.L., Gibbs free energy of gaseous phosphorus dimer. *Chem. Eng. Sci*. 190 (2018) 122. https://doi.org/10.1016/j.ces.2018.06.027

[43] Focsa C., Li H., and Bernath P.F., Characterization of the ground state of Br_2 by laser-induced fluorescence Fourier transform spectroscopy of the B $^3\Pi_{0+u}$ – X $^1\Sigma_g^+$ System, *J. Mol. Spectrosc*. 200 (2000) 104. https://doi.org/10.1006/jmsp.1999.8039

[44] Hajigeorgiou P.G., An extended Lennard-Jones potential energy function for diatomic molecules: Application to ground electronic states. *J. Mol. Spectrosc*. 263 (2010) 101. https://doi.org/10.1016/j.jms.2010.07.003

[45] Abdullah H.Y., A comparative study of potential energy curves with RKRV curves for the ground states of I_2, F_2 and CO molecules. *Bull Mater Sci* 42 (2019) 142. https://doi.org/10.1007/s12034-019-1824-2

[46] Hajigeorgiou P.G., The potential energy function of the ground electronic state of $^{16}O_2$, J. Chem. Phys. 138 (2013) 014309. https://doi.org/10.1063/1.4773285

[47] Ding Q.C., Jia C.S., Liu J.Z., Li J., Du R.F., Liu J.Y., Peng X.L., Wang C.W., and Tang H.X., Prediction of thermodynamic properties for sulfur dimer, Chem. Phys. Lett. 803 (2022) 139844. https://doi.org/10.1016/j.cplett.2022.139844

[48] Li R., Zhang X., Feng W., Jiang Y., Fei D., Jin M., Yan B., and Xu H., Ab initio CI calculations on potential energy curves of low-lying states of BrF and its cation including spin-orbit coupling. Comput. Theor. Chem. 1032 (2014) 20. https://doi.org/10.1016/j.comptc.2014.01.016

[49] Vassilakis A.A., Kalemos A., and Mavridis A., Accurate first principles calculations on chlorine fluoride ClF and its ions $ClF^{\pm}$. *Theor. Chem. Acc.* 133 (2014) 1436. https://doi.org/10.1007/s00214-013-1436-7

[50] Ito F., Sugawara K., Nakanaga T., Takeo H., Matsumura C., Dunham potential coefficients of iodine fluoride. *J. Mol. Spectrosc.* 142 (1990) 191. https://doi.org/10.1016/0022-2852(90)90301-6

[51] Khristenko S.V., Shevelko V.P., Maslov A.I. (1998). Energy Constants of Molecules. In: Molecules and Their Spectroscopic Properties. Springer Series on Atoms+Plasmas, vol 21. Springer, Berlin, Heidelberg. https://doi.org/10.1007/978-3-642-71946-2_3

[52] Reddy RR, Ahmed YN, Gopal KR, Azeem PA, Rao TVR, Dissociation energies of astrophysically important MgO, SO, SiN and TiO from spectroscopic data, J. Quant. Spectrosc. Radiat. Transf. 66 (2000) 501 https://doi.org/10.1016/S0022-4073(99)00182-X

[53] Khairbek, A.A., Interhalogen compounds and polyhalogen ions: Structural diversity, bonding, and applications. Adv. Inorg. Chem. 85 (2025) 91. https://doi.org/10.1016/bs.adioch.2025.07.003

[54] Prior C., Grainger, R.S. Sulfur monoxide: generation, trapping, and synthetic applications. Prog. Heterocycl. Chem. 34 (2023) 1. https://doi.org/10.1016/B978-0-443-18939-5.00014-7

[55] Fernández F.M., Comment on ‘‘Specific heat at constant pressure, enthalpy and Gibbs free energy of boron nitride (BN) using q-deformed exponential-type potential’’ *Phys. B* 739 (2026) 418882. https://doi.org/10.1016/j.physb.2026.418882

[56] Rafi M., Al-Tuwirqi R., Farhan H.., and Khan I.A., A new four-parameter empirical potential energy function for diatomic molecules. *Pramana J. Phys*. 68 (2007) 959. https://doi.org/10.1007/s12043-007-0095-4

[57] H. Bakhti, A. Diaf, M. Hacham, Computing thermodynamic properties of some diatomic molecules using a q-deformed Scarf-like potential, *Mol. Phys*. 120 (2022) e2133752. https://doi.org/10.1080/00268976.2022.2133752.

[58] A. Diaf, M. Hacham, M.M. Ezzine, Thermodynamic properties for some diatomic molecules with the q-deformed hyperbolic barrier potential, *Mol. Phys*. 121 (2023) e2198045. https://doi.org/10.1080/00268976.2023.2198045.

[59] U.E. Ebere, S.A. Ekong, U.S. Okorie, Superstatistical functions of modified shifted Morse potential for diatomic molecules, *Mol. Phys*. 123 (2025) e2423754. https://doi.org/10.1080/00268976.2024.2423754

List of Tables

Table 1: Molecular constants, enthalpy data, and model parameters used in the calculations

Diatomic molecule	Molecular state	Molecular constants			p	Reference-state enthalpies (J mol $^{-1}$) at 298.15 K		η
		r_e (Å)	D_e (cm^{-1})	ω_e (cm^{-1})		H_j^0	$\Delta_f H_j^0$	
Br_2 [43]	X $^1\Sigma_g^+$	2.2810213	15894.546	325.314194	4.4791	12421.1714	30837	2.10
Cl_2 [44]	X $^1\Sigma_g^+$	1.987200	20276.48	559.7507	3.9316	13519.3057	0	2.04
F_2 [45]	X $^1\Sigma_g^+$	1.41193	13408	917.067	4.1296	15326.5040	0	2.01
I_2 [45]	X $^1\Sigma_g^+$	2.66630	12547.34	213.695264472	4.8974	11947.9801	62421	2.00
O_2 [46]	X $^3\Sigma_g^-$	1.20752763	42055.6	1579.833	3.0531	18971.3595	0	0.82
S_2 [47]	X $^1\Sigma_g^+$	1.8920	35993.296	714	3.4741	14280.7796	128600	0.90
BrF [48]	X $^1\Sigma^+$	1.7532	20163.860	669.901	3.8632	14066.1332	-58463	2.51
ClF [49]	X $^1\Sigma^+$	1.6284	21957.7445	786.1	3.6005	14661.1738	-50292	2.10
IF	X $^1\Sigma^+$	1.909757[50]	22699.2293[51]	610.2442 [50]	3.7381	13770.1203	-94759	2.80
SO [52]	X $^3\Sigma^-$	1.48	35150.579	1149.0	3.4993	16587.6431	5007	0.95

Table 2: Calculated and NIST-JANAF [6] values of $\log_{10} K_p$ and RAD for BrF

T (K)	Eq. (22)	NIST [6]	RAD (%)	T (K)	Eq. (22)	NIST [6]	RAD (%)
300	13.122	12.868	1.974	3200	1.446	1.442	0.283
400	9.906	9.906	0.003	3300	1.409	1.404	0.339
500	7.976	7.974	0.019	3400	1.374	1.370	0.264
600	6.688	6.686	0.037	3500	1.340	1.337	0.258
700	5.769	5.765	0.069	3600	1.309	1.306	0.237
800	5.079	5.075	0.084	3700	1.279	1.276	0.269
900	4.543	4.538	0.104	3800	1.251	1.248	0.265
1000	4.113	4.108	0.131	3900	1.225	1.222	0.215
1100	3.762	3.757	0.133	4000	1.199	1.197	0.190
1200	3.469	3.464	0.148	4100	1.175	1.173	0.185
1300	3.221	3.216	0.162	4200	1.152	1.151	0.105
1400	3.009	3.003	0.189	4300	1.130	1.129	0.118
1500	2.824	2.819	0.191	4400	1.109	1.109	0.042
1600	2.663	2.657	0.227	4500	1.090	1.090	0.042
1700	2.521	2.515	0.223	4600	1.071	1.071	0.046
1800	2.394	2.388	0.249	4700	1.052	1.054	0.160
1900	2.281	2.275	0.242	4800	1.035	1.037	0.203
2000	2.178	2.173	0.246	4900	1.018	1.021	0.273
2100	2.086	2.080	0.281	5000	1.002	1.005	0.275
2200	2.002	1.996	0.284	5100	0.987	0.991	0.413
2300	1.925	1.919	0.298	5200	0.972	0.977	0.491
2400	1.854	1.849	0.277	5300	0.958	0.964	0.613
2500	1.789	1.784	0.285	5400	0.945	0.951	0.680
2600	1.729	1.724	0.289	5500	0.932	0.939	0.798
2700	1.673	1.668	0.315	5600	0.919	0.927	0.866
2800	1.621	1.616	0.337	5700	0.907	0.916	0.991
2900	1.573	1.568	0.329	5800	0.895	0.905	1.070
3000	1.528	1.523	0.330	5900	0.884	0.895	1.213
3100	1.486	1.481	0.321	6000	0.873	0.885	1.313

Table 3: Calculated and NIST-JANAF [6] values of $\log_{10} K_p$ and RAD for ClF

T (K)	Eq. (22)	NIST [6]	RAD (%)	T (K)	Eq. (22)	NIST [6]	RAD (%)
300	9.020	9.018	0.017	3200	1.068	1.059	0.818
400	6.830	6.828	0.031	3300	1.042	1.035	0.688
500	5.516	5.513	0.056	3400	1.018	1.012	0.599
600	4.640	4.635	0.104	3500	0.995	0.990	0.540
700	4.014	4.008	0.144	3600	0.974	0.970	0.398
800	3.544	3.538	0.172	3700	0.954	0.952	0.161
900	3.179	3.172	0.211	3800	0.934	0.935	0.079
1000	2.886	2.879	0.254	3900	0.916	0.919	0.331
1100	2.647	2.639	0.302	4000	0.899	0.905	0.710
1200	2.447	2.439	0.347	4100	0.882	0.891	1.006
1300	2.279	2.270	0.378	4200	0.866	0.879	1.446
1400	2.134	2.125	0.412	4300	0.851	0.868	1.927
1500	2.008	1.999	0.459	4400	0.837	0.858	2.453
1600	1.898	1.889	0.489	4500	0.823	0.850	3.143
1700	1.801	1.792	0.511	4600	0.810	0.842	3.775
1800	1.715	1.705	0.574	4700	0.798	0.835	4.464
1900	1.637	1.627	0.642	4800	0.786	0.830	5.329
2000	1.568	1.557	0.692	4900	0.774	0.825	6.143
2100	1.505	1.494	0.715	5000	0.763	0.822	7.135
2200	1.447	1.437	0.713	5100	0.753	0.819	8.079
2300	1.395	1.384	0.776	5200	0.743	0.817	9.089
2400	1.347	1.336	0.789	5300	0.733	0.817	10.274
2500	1.302	1.291	0.862	5400	0.724	0.817	11.412
2600	1.261	1.250	0.886	5500	0.715	0.818	12.613
2700	1.223	1.212	0.908	5600	0.706	0.820	13.873
2800	1.188	1.177	0.901	5700	0.698	0.822	15.088
2900	1.155	1.144	0.926	5800	0.690	0.825	16.360
3000	1.124	1.114	0.873	5900	0.682	0.830	17.785
3100	1.095	1.086	0.811	6000	0.675	0.834	19.063

Table 4: Calculated and NIST-JANAF [6] values of $\log_{10} K_p$ and RAD for IF

T (K)	Eq. (22)	NIST [6]	RAD (%)	T (K)	Eq. (22)	NIST [6]	RAD (%)
300	22.168	20.512	8.075	3200	2.265	2.278	0.572
400	16.685	16.331	2.166	3300	2.201	2.215	0.612
500	13.394	13.397	0.021	3400	2.142	2.155	0.622
600	11.200	11.203	0.025	3500	2.085	2.098	0.613
700	9.633	9.637	0.043	3600	2.032	2.045	0.647
800	8.457	8.462	0.057	3700	1.981	1.994	0.638
900	7.543	7.548	0.072	3800	1.933	1.947	0.698
1000	6.811	6.818	0.106	3900	1.888	1.901	0.683
1100	6.212	6.220	0.130	4000	1.845	1.859	0.760
1200	5.713	5.722	0.162	4100	1.804	1.818	0.779
1300	5.290	5.300	0.185	4200	1.765	1.779	0.799
1400	4.928	4.939	0.224	4300	1.728	1.743	0.886
1500	4.614	4.626	0.263	4400	1.692	1.708	0.934
1600	4.339	4.352	0.302	4500	1.658	1.675	1.006
1700	4.096	4.110	0.338	4600	1.626	1.643	1.049
1800	3.880	3.895	0.380	4700	1.595	1.613	1.129
1900	3.687	3.702	0.408	4800	1.565	1.585	1.252
2000	3.513	3.528	0.432	4900	1.537	1.558	1.363
2100	3.355	3.371	0.472	5000	1.510	1.532	1.465
2200	3.212	3.227	0.477	5100	1.483	1.507	1.561
2300	3.080	3.096	0.501	5200	1.458	1.483	1.656
2400	2.960	2.976	0.532	5300	1.434	1.461	1.820
2500	2.849	2.865	0.547	5400	1.411	1.439	1.924
2600	2.747	2.762	0.547	5500	1.389	1.419	2.105
2700	2.652	2.667	0.564	5600	1.368	1.399	2.232
2800	2.564	2.578	0.555	5700	1.347	1.380	2.374
2900	2.481	2.496	0.584	5800	1.327	1.362	2.536
3000	2.405	2.419	0.598	5900	1.308	1.345	2.720
3100	2.333	2.346	0.574	6000	1.290	1.329	2.930

Table 5: Calculated and NIST-JANAF [6] values of $\log_{10} K_p$ and RAD for SO

T (K)	Eq. (22)	NIST [6]	RAD (%)	T (K)	Eq. (22)	NIST [6]	RAD (%)
300	10.593	3.689	187.144	3200	1.235	1.225	0.790
400	8.012	3.880	106.484	3300	1.205	1.196	0.784
500	6.463	3.906	65.454	3400	1.178	1.168	0.840
600	5.430	3.887	39.693	3500	1.152	1.142	0.860
700	4.692	3.851	21.843	3600	1.127	1.117	0.920
800	4.139	3.811	8.603	3700	1.104	1.094	0.920
900	3.709	3.708	0.014	3800	1.082	1.071	1.034
1000	3.364	3.363	0.036	3900	1.061	1.050	1.068
1100	3.083	3.081	0.050	4000	1.041	1.030	1.107
1200	2.848	2.846	0.064	4100	1.023	1.011	1.144
1300	2.649	2.647	0.083	4200	1.005	0.993	1.170
1400	2.479	2.476	0.120	4300	0.988	0.976	1.180
1500	2.331	2.328	0.148	4400	0.971	0.959	1.272
1600	2.202	2.199	0.153	4500	0.956	0.944	1.229
1700	2.088	2.084	0.215	4600	0.941	0.928	1.368
1800	1.987	1.983	0.214	4700	0.926	0.914	1.359
1900	1.897	1.892	0.247	4800	0.913	0.900	1.416
2000	1.815	1.810	0.286	4900	0.900	0.887	1.424
2100	1.741	1.736	0.313	5000	0.887	0.874	1.492
2200	1.674	1.668	0.384	5100	0.875	0.862	1.503
2300	1.613	1.607	0.386	5200	0.863	0.850	1.569
2400	1.557	1.550	0.458	5300	0.852	0.838	1.689
2500	1.506	1.498	0.501	5400	0.841	0.827	1.741
2600	1.458	1.450	0.543	5500	0.831	0.816	1.842
2700	1.414	1.406	0.553	5600	0.821	0.806	1.866
2800	1.373	1.365	0.574	5700	0.811	0.796	1.935
2900	1.335	1.326	0.657	5800	0.802	0.787	1.918
3000	1.299	1.290	0.709	5900	0.793	0.777	2.074
3100	1.266	1.257	0.706	6000	0.784	0.768	2.140

List of Figures

Figure 1: Variation of $\log_{10} K_p$ and relative absolute deviation (RAD) with temperature for BrF: The upper panel compares the qHIP results with NIST-JANAF data [6], while the lower panel shows the corresponding RAD values

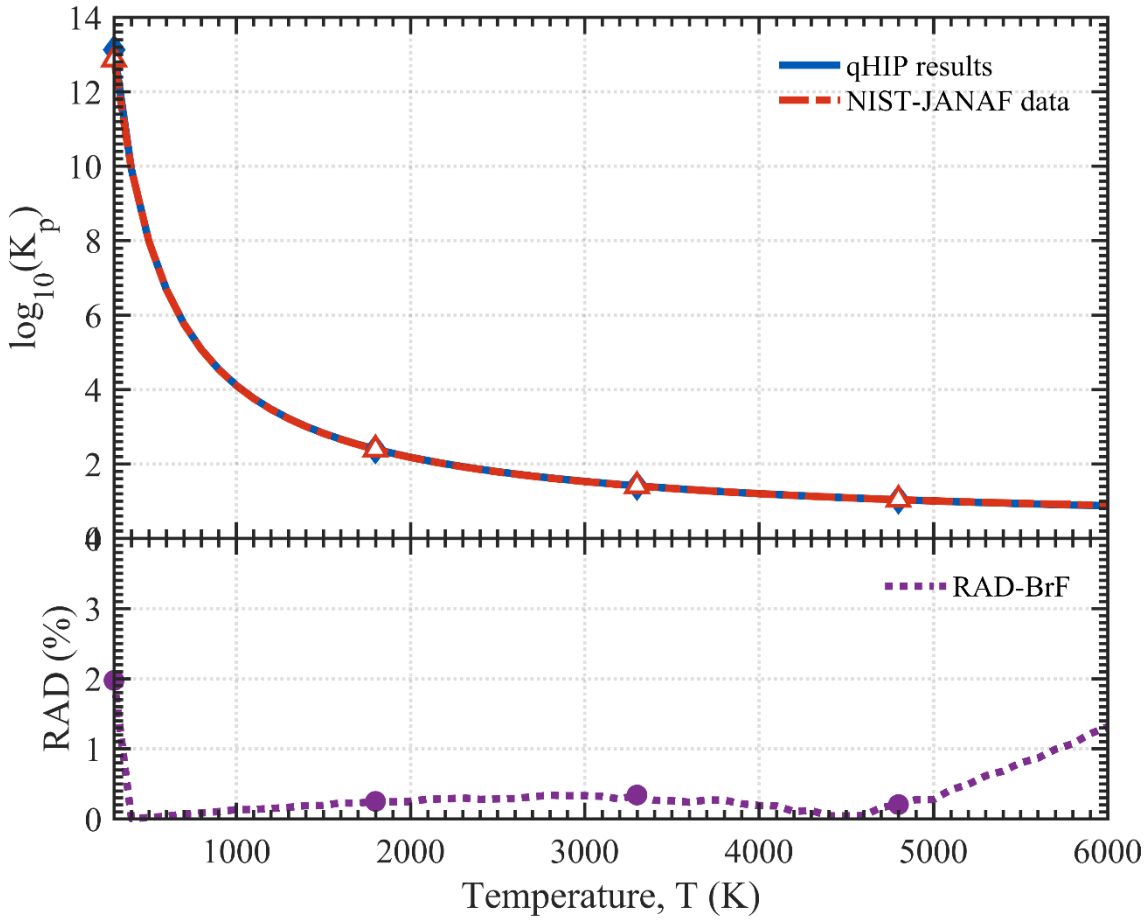


Figure 2: Variation of $\log_{10} K_p$ and relative absolute deviation (RAD) with temperature for ClF: The upper panel compares the qHIP results with NIST-JANAF data [6], while the lower panel shows the corresponding RAD values

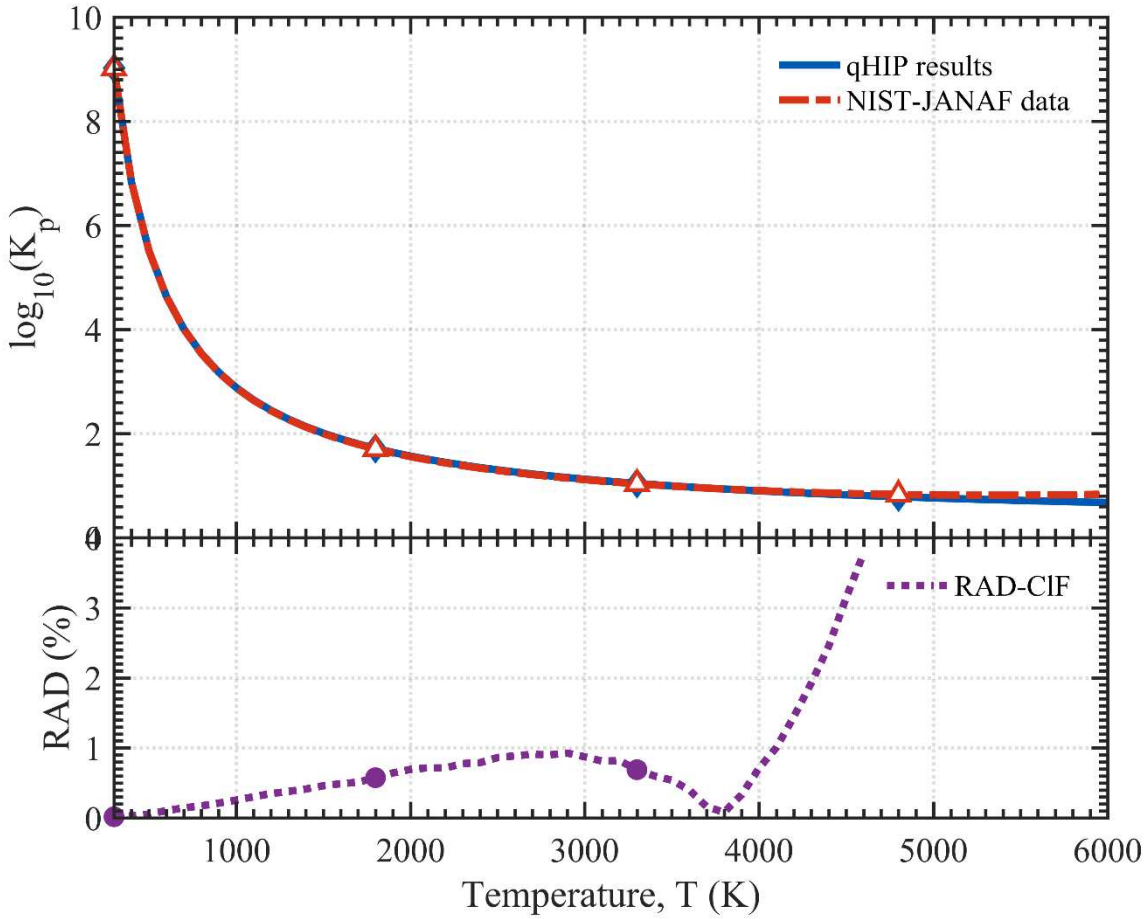


Figure 3: Variation of $\log_{10} K_p$ and relative absolute deviation (RAD) with temperature for IF: The upper panel compares the qHIP results with NIST-JANAF data [6], while the lower panel shows the corresponding RAD values

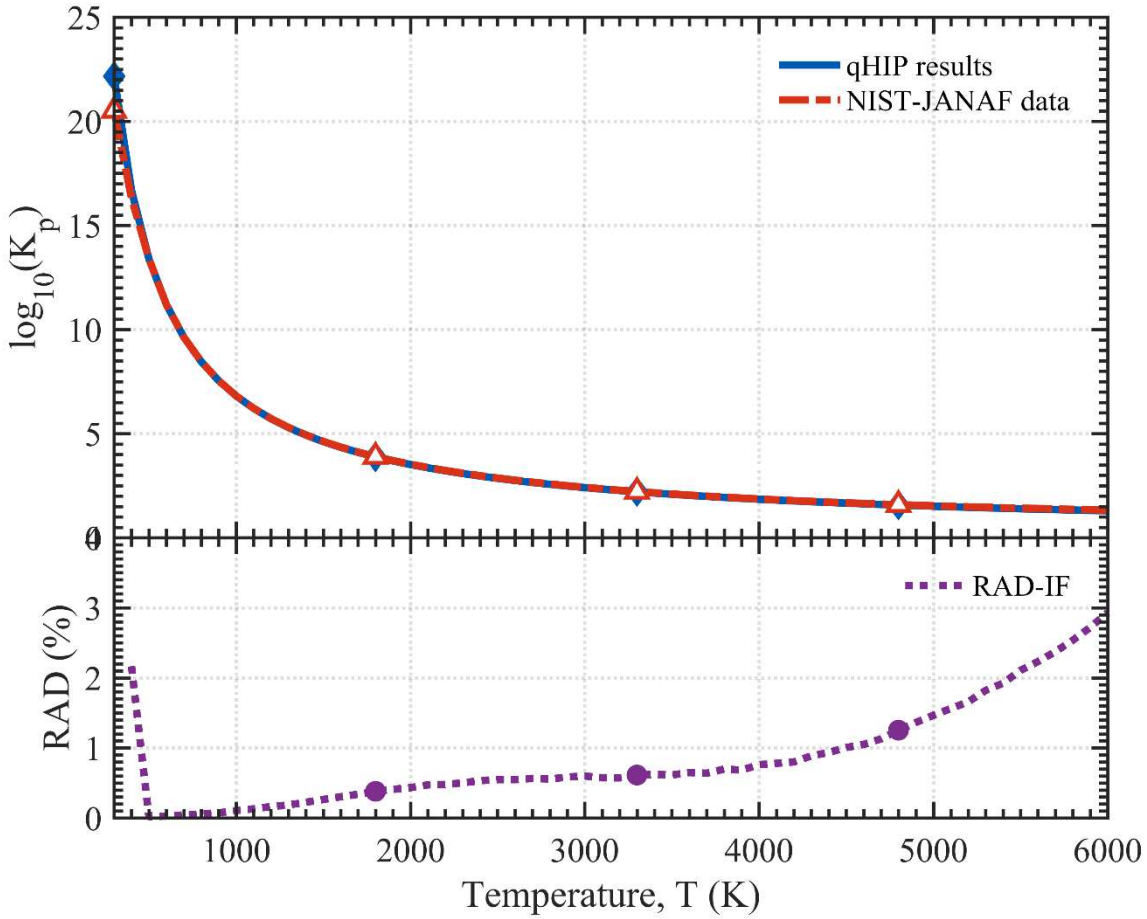


Figure 4: Variation of $\log_{10} K_p$ and relative absolute deviation (RAD) with temperature for SO: The upper panel compares the qHIP results with NIST-JANAF data [6], while the lower panel shows the corresponding RAD values

